Available online at www.sciencedirect.com
SCIENCE DIRECT
Journal of Catalysis 239 (2006) 125–136
JOURNAL OF CATALYSIS
www.elsevier.com/locate/jcat

Structure and catalytic properties of vanadium oxide supported on mesocellulous silica foams (MCF) for the oxidative dehydrogenation of propane to propylene

Yong-Mei Liu [a], Wei-Liang Feng [a], Ting-Cheng Li [b], He-Yong He [a], Wei-Lin Dai [a], Wei Huang [b], Yong Cao [a,*], Kang-Nian Fan [a]

[a] *Department of Chemistry & Shanghai Key Laboratory of Molecular Catalysis and Innovative Materials, Fudan University, Shanghai 200433, PR China*
[b] *Laboratory of Advanced Materials, Fudan University, Shanghai 200234, PR China*

Received 1 November 2005; revised 21 December 2005; accepted 21 December 2005

Available online 14 February 2006

Abstract

A series of vanadium containing mesocellular silica foams (MCF) featuring a well-defined three-dimensional (3D) mesoporosity with ultralarge mesopores were studied with regard to their performance in the oxidative dehydrogenation (ODH) of propane. Catalysts supported on two-dimensional hexagonally ordered siliceous SBA-15 and MCM-41, as well as conventional amorphous silica, were also examined. The dispersity and the nature of the vanadium oxide species were characterized by means of DRIFTS, Raman spectroscopy, DR UV–vis, and H_2-TPR. Textural, SAXS, and TEM results indicate that the characteristic mesocellular structural features of MCFs are preserved after the vanadium incorporation. Spectroscopic measurements show that vanadium exists mainly in a tetrahedral environment in dehydrated V-MCF catalysts with V content <4.2 wt%, indicating that a very high surface concentration of isolated or low-polymeric VO_x species could be achieved on the present V-MCF systems. The MCF-supported vanadia catalysts exhibit much higher propane conversion and propylene productivity than their conventional V-SBA, V-MCM, and V–SiO_2 counterparts in the ODH of propane, demonstrating that apart from the active redox sites, internal molecular transport in mesopores of the catalyst also plays an important role in the gas-phase selective oxidation reactions.

Keywords: Supported vanadia catalyst; Mesocellular silica foams; Oxidative hydrogenation of propane; Propylene; Internal molecular transport

1. Introduction

Propylene is a major building block of the petrochemical industry and is used for the production of diverse products, ranging from solvents to plastics. Currently, propylene is produced mainly by steam cracking or direct dehydrogenation (DH) of various hydrocarbon feedstocks at high temperatures, where intensive energy consumption and coking present serious problems [1,2]. With the propylene market growing at 4–5% per year [3] and fuel costs constantly rising, considerable research efforts have been focused on the development of less energy-intensive processes for the production of propylene [4–6].

The catalytic oxidative dehydrogenation (ODH) of propane is an attractive alternative route for the production of propylene that is thermodynamically favored at much lower temperatures and usually does not lead to the formation of coke and smaller hydrocarbons [4]. But this selective oxidation is particularly challenging, given the high reactivity of propylene toward further oxidation [5,6]. Recent literature has focused on the design and development of selective catalysts that can allow the effective transformation of propane at lower temperatures. The most selective catalysts reported in the recent literature consist of V–Mg–O, V–Nb–O, V–Zr–Si–O, $NiMoO_4$, K–Mo–Si–Ti–O, and V-silicate [7–14]. In particular, promising results have been obtained when vanadia-based catalysts are promoted or dispersed on various supports with a high surface area [8,14].

Recently, the new discovery of the family of siliceous mesostructured materials, generally denoted as M41S, has

* Corresponding author. Fax: +86 21 65642978.
E-mail address: yongcao@fudan.edu.cn (Y. Cao).

0021-9517/$ – see front matter
doi:10.1016/j.jcat.2005.12.028

opened new and exciting opportunities in the field of separation and catalysis [15,16]. These mesoporous materials usually exhibit great versatility in terms of both chemical nature and structural properties, and thus the synthesis, characterization, and catalytic properties of V-containing mesoporous silica have been extensively reported. Peña et al. [17] and Buyevskaya et al. [18] developed various synthetic methods, including one-pot synthesis and grafting, for the synthesis of a range of V-containing mesoporous MCM-41 and MCM-48 catalysts with controlled site isolation for the selective oxidation of propane to propylene. Solsona et al. [19] showed that the conventional impregnation method is more convenient and practical for obtaining the highly active and selective VO_x/MCM-41 catalysts with a higher concentration of isolated VO_x species. Compared with the conventional amorphous SiO_2-supported vanadia catalysts, these V-containing MCM materials were found to be more active and selective for the ODH of propane [19,20]. The notable difference in propane ODH behavior has been explained by taking into account that the higher surface area of MCM materials can allow better dispersion of active V species on the mesoporous supports [18–20]. However, to the best of our knowledge, single-pass propylene yields >20% have rarely been achieved over these V-containing MCM materials [17–20].

In an effort to develop more suitable ODH catalysts, we have recently reported that using mesoporous SBA-15 silica as a support can allow the generation of a new type of highly efficient V-containing SBA-15 catalyst exhibiting high selectivity (80%) to olefins at high propane conversion (42%) in the ODH of propane, which is found to be more active and selective with respect to V-MCM catalysts [21–23]. The enhanced propylene selectivity at higher propane conversion achievable over the V-containing SBA-15 catalysts has been attributed to the larger pore diameters and the lower surface acidity of the SBA-15 materials, which can provide more favorable conditions for mass transfer, thereby leading to enhanced performance for ODH of propane compared with their conventional MCM counterparts [23]. However, the catalytic results in terms of propylene productivity (i.e., the space-time yield for propylene production) achieved over the highly active V-SBA-15 catalysts are still far from being of industrial interest.

Unlike MCM-41 and SBA-15, which have two-dimensional mesopore structures, mesocellular silica foams (MCF) is a new class of three-dimensional (3D) hydrothermally robust materials with ultra-large mesopores (up to 50 nm) [24–26]. In terms of the textural and framework structure, the MCF materials resemble aerogels and are composed of uniform spherical cells interconnected by windows with a narrow size distribution [24]. Given their 3D mesopore system with pore sizes substantially larger than those of any other mesostructures, MCF materials are known to have advantages over their more ordered counterparts MCM-41 or SBA-15 in terms of better diffusion of reactants and products, allowing them to better overcome mass transfer limitations [26,27]. Despite MCF's important potential uses in catalytic applications, reports in the literature dealing with the catalytic utilization of transition elements incorporating MCF-type materials are rare [28–30].

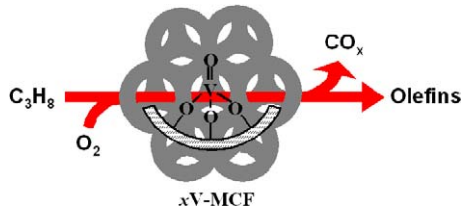

Scheme 1. Oxidative dehydrogenation of propane over highly dispersed vanadia supported on mesostructured cellular silica foam (MCF).

In this study, we report the development of a new efficient mesoporous V-containing MCF silica catalyst system featuring a well-defined 3D, continuous, ultra-large mesopore structure (Scheme 1) exhibiting very high propylene productivity for the ODH of propane. The effect of vanadium loading and impact of the silica support structure on the performance of the V-containing materials are discussed in the light of detailed characterization of the physicochemical properties of the catalysts by N_2 adsorption, SAXS, TEM, DRIFTS, DR UV–vis, Raman spectroscopy, and H_2-TPR.

2. Experimental

2.1. Catalyst preparation

The purely siliceous MCF sample was prepared as described previously [25] using a Pluronic P123 triblock copolymer ($EO_{20}PO_{70}EO_{20}$, M_{av} = 5800, Aldrich) surfactant with 1,3,5-trimethylbenzene (TMB) as the organic swelling agent with TMB/P123 = 0.5 (w/w). In a typical preparation, a solution of P123:TMB:1.6 M HCl:TEOS = 2:1:75:4.25 (mass ratio) was prepared at room temperature, then heated to 40 °C. After 24 h at 40 °C, the milky reaction mixture was transferred to an autoclave and aged at 100 °C for another 24 h. The solid products were filtered off and dried overnight at 100 °C under static conditions. The occluded surfactant was removed by calcination at 600 °C for 5 h in air, yielding the final mesoporous MCF material.

MCF-supported vanadia catalysts were prepared by an alcoholic impregnation method as described previously [23]. A methanol solution of NH_4VO_3 to achieve a final V content of 1.4–5.6 wt% of V atoms was contacted with the MCF carrier at 60 °C, and the methanol was rotaevaporated until complete dryness. Then the catalysts were dried overnight in air at 120 °C, followed by calcination at 600 °C for 4 h in air. The impregnated samples, denoted by numbers (representing the V content in the calcined catalysts) followed by MCF, are summarized in Table 1. For example, the sample designated 2.8V-MCF is an MCF-supported catalyst with 2.8 wt% of V atoms. For comparison, vanadia catalysts supported on SBA-15, MCM-41, and amorphous silica (Shanghai Super Chemical Material Co. Ltd., B type, 320 $m^2\,g^{-1}$) were also been prepared following the same procedure.

2.2. Catalyst characterization

Nitrogen adsorption and desorption at 77 K were measured using a Micromeritics TriStar 3000 after the samples were de-

Table 1
Characteristics of the mesoporous silica supported vanadia catalysts

Sample	V-density (VO_x per nm^2)	S_{BET} ($m^2\,g^{-1}$)	V_p ($cm^3\,g^{-1}$)	D_S[a] (nm)	D_C[b] (nm)	D_W[b] (nm)	Absorption edge energy (eV)
MCF	–	660	1.54	24.5	22.1	7.3	–
1.4V-MCF	0.30	552	1.18	22.5	18.3	4.4	3.27
2.8V-MCF	0.66	504	1.14	21.1	18.1	4.1	2.94
4.2V-MCF	1.08	457	1.02	20.8	17.6	3.6	2.84
5.6V-MCF	1.61	412	0.94	20.8	17.2	3.3	2.33
2.8V-SBA	0.69	478	0.88	–	6.4	–	2.58
4.5V-MCM	0.65	820	0.46	–	2.5	–	2.28
1.8V-SiO_2	0.71	300	0.67	–	16.1	–	2.32

[a] Sphere diameter, D_S, determined from small-angle X-ray scattering analyses [36].
[b] Cell diameter, D_C, and window diameter, D_W, determined according to the BJH method.

gassed (1.33×10^{-2} Pa) at 300 °C overnight. The specific surface area was calculated using the BET method, and pore size distribution was determined by the BJH method.

Small-angle X-ray scattering (SAXS) experiments were performed on a Germany Bruker NanoSTAR U SAXS system equipped with high-resolution pinhole chamber using Cu-K_α radiation ($\lambda = 1.518$ Å) and a 106-cm sample-to-detector distance. Transmission electron microscopy (TEM) images were recorded digitally with a Gatan slow-scan charge-coupled device camera on a JEOL 2011 electron microscope operating at 200 kV. The samples were prepared by dispersing the powder products as a slurry in acetone, which was then deposited and dried on a holey carbon film on a Cu grid.

Diffuse reflectance infrared Fourier transform spectroscopy (DRIFTS) characterization of the catalysts was performed using a Bruker Vector 22 instrument equipped with a DTGS detector and a KBr beam splitter [31]. The samples were placed in a sample cup inside a Harrick diffuse reflectance cell equipped with ZnSe windows and a thermocouple mount that allowed direct measurement of the sample temperature. All spectra were collected in dry air atmosphere at 200 °C.

In situ laser Raman spectra were obtained using a confocal microprobe Jobin Yvon Lab Ram Infinity Raman system equipped with both visible and UV excitation lines. The visible Raman measurements were carried out using internal Ar^+ excitation at 514.5 nm with a power of 10 mW. The sample was loaded in an in situ cell and was pretreated in dry airflow at 500 °C for 1 h for dehydration. All spectra were recorded at 200 °C in N_2 gas flow with a resolution of 4 cm^{-1}. The UV-Raman measurements were carried out using the UV line at 325 nm from a Kimmon IK3201R-F He–Cd laser as the exciting source, with a laser output of 30 mW and a maximum incident power at the sample of approximately 6 mW.

Diffuse reflectance UV–vis spectra were collected on a Varian Cary 5 spectrophotometer equipped with a "Praying Mantis" attachment from Harrick. The sample cell was equipped with a heater unit, a thermocouple, and a gas flow system for in situ measurements. The samples were dehydrated in situ in dry air at 550 °C for 4 h. The spectra were recorded after cooling to room temperature, with dry air flowed through the sample to avoid rehydration. The absorption edge energy values were determined from the energy intercept of a linear fit passing through the near-edge region in a plot of $[F(R_\infty) \cdot h\nu]^{1/2}$ vs $h\nu$, where the first parameter refers to the Kubelka–Munk function and $h\nu$ is energy of the incident photon [32–34].

Temperature-programmed reduction (TPR) spectra were obtained on a homemade apparatus loaded with 100 mg of catalyst [33]. The samples were pretreated in flowing air at 600 °C for 2 h to ensure complete oxidation, and then the samples were cooled to room temperature in argon. The samples were subsequently contacted with an H_2/Ar mixture (H_2/Ar molar ratio of 5/95 and a total flow of 40 ml min^{-1}), then heated, at a rate of 10 °C min^{-1}, to a final temperature of 800 °C. H_2 consumption was monitored using a thermal conductivity detector.

2.3. Catalytic tests

The catalytic properties of the samples were investigated in a fixed-bed quartz tubular flow reactor (6 mm i.d., 400 mm long) equipped with several gas flow lines with mass flow controllers to supply the feed, consisting of a mixture of propane/oxygen/nitrogen with a molar ratio of 1/1/8. The temperature in the middle of the catalytic bed was measured with a coaxial thermocouple. Catalyst samples (60–80 mesh) were introduced into the reactor and diluted with 300 mg of quartz powder (40–60 mesh) to maintain a constant volume in the catalyst bed. In the present study, gas hourly space velocity (GHSV) and space-time yield (STY) of propylene production are related to the catalyst weight. To obtain different propane conversion levels at constant reaction temperature (550 °C), the GHSV was varied from 10,000 to 180,000 L kg_{cat}^{-1} h^{-1}. The feed and the reaction products were analyzed on-line by a gas chromatograph (type GC-122, Shanghai). Permanent gases (O_2, CO, and CO_2) were separated using a TDX-01 column connected to a thermal conductivity detector, and other reaction products were analyzed using a Porapak Q column connected to a flame ionization detector. Blank runs showed that under the experimental conditions used in this work, the homogeneous reaction could be neglected.

3. Results

3.1. Catalyst characterization

The as-prepared MCF-supported vanadia samples were analyzed using SAXS. X-ray scattering is observed if uniformly

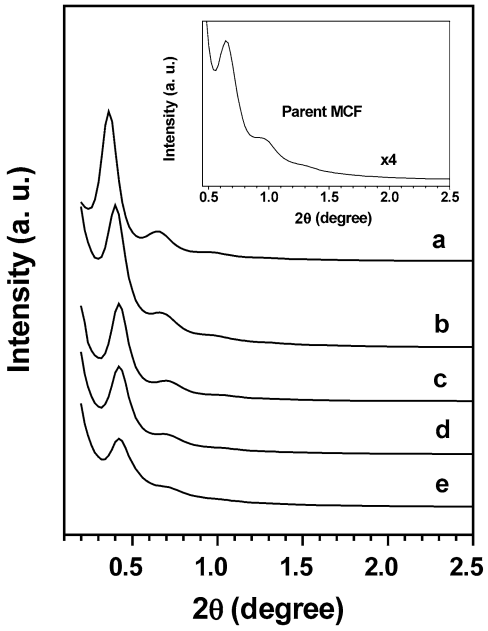

Fig. 1. Small-angle X-ray scattering patterns of calcined MCF-supported vanadia catalysts: (a) MCF; (b) 1.4V-MCF; (c) 2.8V-MCF; (d) 4.2V-MCF; (e) 5.6V-MCF.

sized particles are present, as opposed to X-ray diffraction associated with periodic structures [35]. Fig. 1 shows the recorded SAXS data for the V-MCF samples with V loadings ranging from 1.4 to 5.6 wt%. The scattering pattern of the parent MCF material is well resolved and shows one strong primary peak and two higher-order peaks with exponentially decreasing intensities. The occurrence of the higher-order peaks is an indication of the narrow size distribution of the spherical cells [36]. The sphere diameters, D_S, determined from SAXS data, are given in Table 1 for MCF samples with various V loadings. The D_S values agree with the cell diameters, D_C, derived from nitrogen sorption, and with the cell sizes obtained from TEM. As observed previously for V-SBA systems, on low-angle X-ray diffraction [23], a slight shift of the primary peak to higher 2θ values, with a corresponding decrease in the peak intensity with increasing vanadium loading for the V-MCF samples, were also noted. The shift of the primary peak to higher scattering angles can be taken as an indication of a slight decrease in the sphere diameters, possibly due to a contraction of their frameworks with increasing vanadium loading during the calcination procedure. The reduction of the scatterings may be caused by a partial structural collapse of the MCF pores [35]. However, the mesocellular arrangement of the MCF frameworks was still well retained after incorporation of vanadia, as can be seen from the TEM and N_2 adsorption data.

TEM images (Figs. 2a and 2b) of all MCF materials (including the V-containing samples) revealed a disordered array of silica struts composed of uniform-sized spherical cells (18–24 nm) interconnected by windows with a narrow size distribution, which is the characteristic structural feature of the MCF materials [24,35]. A schematic of the strutlike structure, given in Scheme 1, shows the cells of the MCF structure framed by the silica struts. Note that this strutlike structure of MCF materials resembles aerogels [35]. The cell sizes estimated from TEM are consistent with the cell sizes as determined from nitrogen sorption (D_C), given in Table 1. The wall thickness of the MCFs estimated by TEM is ∼4–6 nm, in agreement with the thick, robust framework walls observed in acid-synthesized MCF-type mesoporous silica as reported in the literature [35]. TEM analyses indicate that the continuous 3D pore structure of the MCF is robust enough to survive the vanadium incorporation process and so offers an excellent matrix to support highly dispersed vanadium species.

The maintenance of the well-defined MCF frameworks after introduction of vanadium is further supported by the nitrogen

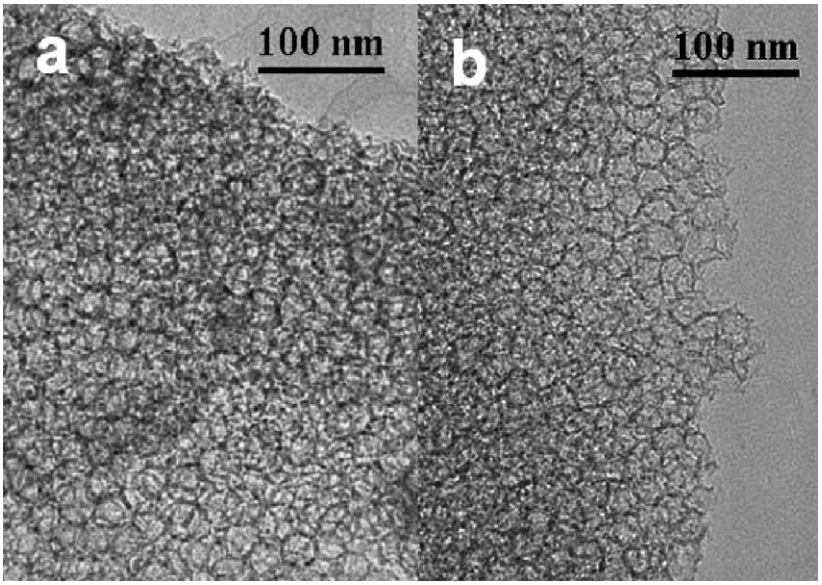

Fig. 2. Representative TEM images of (a) as-prepared parent MCF and (b) 2.8V-MCF showing an open mesocellular structure.

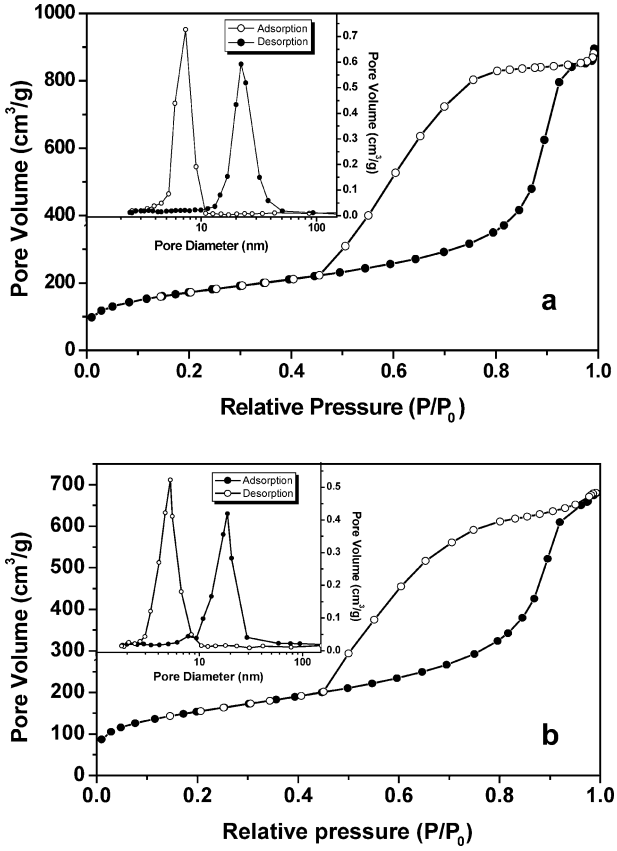

Fig. 3. Nitrogen sorption isotherms for (a) as-prepared parent MCF; (b) 2.8V-MCF. Inset shows the pore size distribution (PSD) of the corresponding samples.

sorption data. The nitrogen adsorption/desorption isotherms (Fig. 3) are of type IV and show steep hysteresis of type H1 at high relative pressures. The pore size distribution of the sample 2.8V-MCF shown in the inset of Fig. 3b unambiguously reveals that the 3D mesocellular structure of the support has been preserved. The S_{BET} of the vanadium-containing samples is lower than that of the unloaded supports and decreases with increasing VO_x loading. This decreasing trend is also demonstrated by the data for the cell and window sizes. The results in Table 1 also clearly indicate that the introduction of vanadium would cause a continuous loss of the pore volume of the MCF materials, but nonetheless it would remain significantly higher than the pore volume of V-containing materials prepared using SBA-15 and MCM-41. Thus, it can be concluded that the ultra-large mesoporous MCF catalysts with a high surface area and extremely high pore volume (>0.9 cm^3 g^{-1}) could be obtained at all V loadings in the present study.

DRIFTS was used to follow the variation behavior of the hydroxyl groups present on the surface of the V-MCF samples as a function of vanadium loading. As shown in Fig. 4, the spectrum in the hydroxyl region of the pure siliceous MCF support displays a narrow vibration band at 3740 cm^{-1} attributed to isolated terminal silanol groups and a broad absorption band at 3700–3300 cm^{-1} (centered at ca. 3660 cm^{-1}) due to OH-stretching vibrations of geminal and associated terminal silanol groups located on the pore walls of the support [37]. The rapid

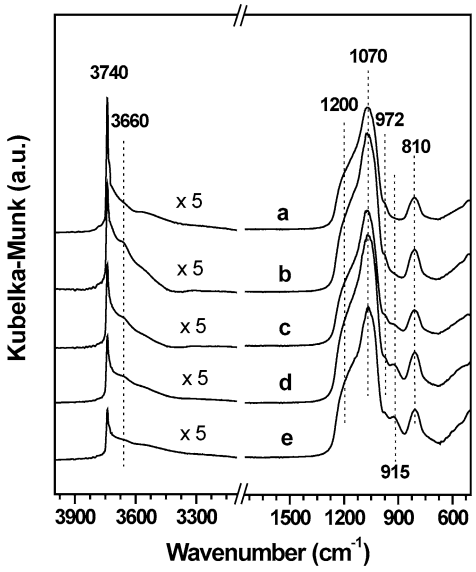

Fig. 4. FTIR spectra of the V-MCF catalysts containing different amounts of vanadium: (a) MCF; (b) 1.4V-MCF; (c) 2.8V-MCF; (d) 4.2V-MCF; (e) 5.6V-MCF.

decrease in the intensity of the isolated terminal silanol groups with increasing vanadium loading indicates that the anchoring of vanadium oxide species on to the MCF surface is accompanied by a simultaneous consumption of the isolated terminal silanol groups [22,23]. This observation is consistent with results for the vanadium-immobilized MCM silica system recently reported by Stucky et al. [38].

Fig. 4 also presents the DRIFTS spectra in the skeletal region of 2000–650 cm^{-1} for the V-loaded MCF materials. As shown in the spectrum of the parent MCF silica, the typical bands due to siliceous Si–O–Si material are observed: a main band at 1070 cm^{-1} with a shoulder at 1200 cm^{-1}, due to asymmetric Si–O–Si stretching modes, the corresponding symmetric stretch at 810 cm^{-1}, and Si–O– or Si–OH at 972 cm^{-1} [39]. In the spectra of the V-containing samples, an additional band at ca. 915 cm^{-1}, indicative of Si–O–V species [38], is well developed for the samples with a V content up to 5.6 wt%. Coupled with the significant spectral changes in the hydroxyl region, these phenomena further confirm the perturbed silica vibrations due to the incorporation of vanadium into the MCF silica framework; other researchers have reported similar trends in the IR spectra of their catalytic vanadia-silicas [40–42].

Laser Raman spectroscopy was used to elucidate the molecular nature of the vanadium species dispersed on the MCF materials. Fig. 5, spectrum a, shows the visible Raman spectrum of the pure siliceous MCF, which exhibits spectroscopic features similar to those of amorphous SiO_2 [43]. As shown in Fig. 5, spectra b–d, Raman bands at 214, 298, 490, 680, and 1036 cm^{-1} are observed for the V-MCF samples with V content <4.2 wt%. When the vanadium content in the sample is 5.6 wt%, six additional bands, at 283, 405, 690, and 991 cm^{-1}, characteristic of crystalline V_2O_5, are detected. Bands at 214 and 480 cm^{-1} are associated with the vibration of the siloxane rings of siliceous MCF [44]. The weak feature centered at 680 cm^{-1} can be assigned to the stretching and bending modes

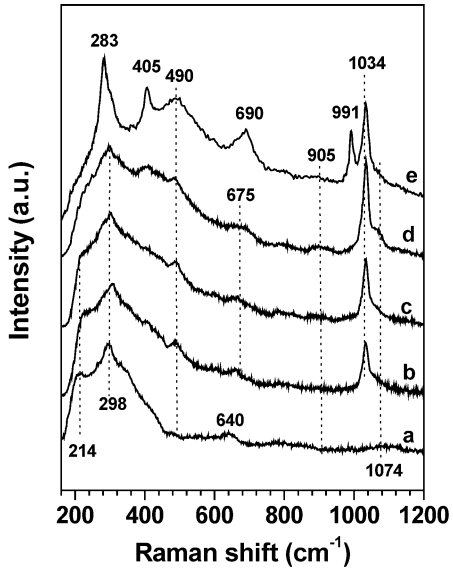

Fig. 5. Visible Raman spectra of the V-MCF catalysts containing different amounts of vanadium: (a) MCF; (b) 1.4V-MCF; (c) 2.8V-MCF; (d) 4.2V-MCF; (e) 5.6V-MCF.

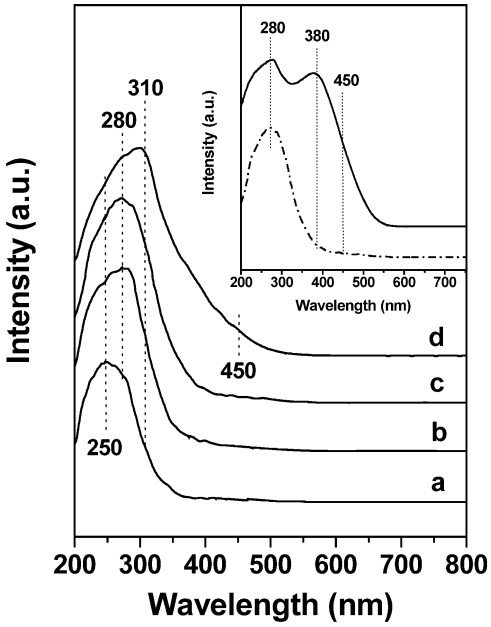

Fig. 6. Diffuse reflectance UV–vis spectra of calcined vanadia catalysts after dehydration at 550 °C in air for 4 h: (a) 1.4V-MCF; (b) 2.8V-MCF; (c) 4.2V-MCF; (d) 5.6V-MCF. Inset shows the hydrated (—) and dehydrated (- - -) spectra of the 4.2V-MCF catalyst.

of V–O bonds; a series of bands in this region has been identified for model complex $OV[OSi(OtBu)_3]_3$ [45]. The band at ~675 cm^{-1} also may be attributed to stretching motions of oxygen in a bridging position between three vanadium atoms (OV_3), in accordance with previous results [46]. These results therefore suggest that the weak band at 675 cm^{-1} observed for the V-MCF samples with V content <4.2 wt% is related to a small number of polymeric vanadia species. The band at 1034 cm^{-1} is attributed to the symmetric stretching mode of the V=O bond of the isolated tetrahedral VO_4 species, as illustrated in Scheme 1 [23,45,47]. The Raman bands at 905 and 1074 cm^{-1} are characteristic of Si–O– and Si(–O–)$_2$ functionalities [48], which have been assigned to perturbed silica vibrations that are indicative of the formation of V–O–Si bonds [49]. The absence of a typical band at ca. 991 cm^{-1} of V_2O_5 in Fig. 5, spectra b–d, implies that no crystalline V_2O_5 is formed in V-MCF samples with V content <4.2 wt%. This suggests that the vanadium species in V-MCF samples are isolated, or at least highly dispersed, on the surface of the MCF materials [22,23,49].

For the 5.6V-MCF sample, an additional shoulder band at ca. 991 cm^{-1} appears, indicating that at this loading (~5.6 wt% of V), vanadium centers aggregate to form crystallites of V_2O_5 that can be observed by Raman spectroscopy. According to a recent investigation by Iglesia et al. [50], the ratio of scattering cross-sections for bulk V_2O_5 and isolated tetrahedral VO_4 has been estimated to be 10. Using this ratio of Raman cross-sections and assuming that only V_2O_5 crystallites and isolated VO_4 species are present, the ratio of V_2O_5:VO_4 for the 5.6 wt% V-MCF sample is estimated to be 0.04. The VO_x concentrations at which V_2O_5 is observed (>1.1 VO_x nm^{-2}; see Table 1) are well below those required for a monolayer of polymeric vanadia (~10 VO_x nm^{-2}), calculated on the basis of the literature value for the cross-sectional area of a $VO_{5/2}$ group of 0.103 nm^2 [51]. This indicates that the VO_x surface species tend to form larger clusters when a certain VO_x concentration is reached. Recently, similar behavior was observed for SBA-15- and MCM-41-supported vanadia, although the formation of crystalline V_2O_5 was observed at even lower concentrations (<0.69 VO_x nm^{-2}) than for VO_x/MCF [19,23,37]. This demonstrates that a much higher dispersion and isolation of the active V species fully accessible to the reaction molecules can be achieved on the V-containing MCF materials compared with conventional silica supports.

Additional structural information on the surface VO_x species can be obtained from UV–vis diffuse reflectance measurements. It is known that the energy of the oxygen → vanadium charge-transfer (CT) bands serves as a good indicator for the coordination of the central V^{5+} center. In general, with increasing coordination number, a shift in the CT band to lower energy (i.e., higher wavelength) is observed [49,52–54]. Fig. 6 shows the diffuse reflectance UV–vis spectra of the dehydrated MCF-supported vanadia samples, showing a red shift of the longest-wavelength CT band with increasing vanadium content. As discussed later in the paper, a comparing the band maxima of the present V-MCF samples or conventional V-containing siliceous materials with those of vanadium reference compounds can enable more accurate assignment of the molecular structures of vanadia on MCF. The absorption maximum of model compound $OV[OSi(OtBu)_3]_3$ was measured at 250 nm [45]. In $Mg_3V_2O_8$, the monomeric vanadium ion is tetrahedrally coordinated with band maxima at 260/303 nm [55]. NH_4VO_3 and $NaVO_3$ both consist of polymerized VO_4 units and give rise to band maxima at 288/363 and 281/353 nm, respectively [56,57]. In crystalline V_2O_5, vanadium is located in the center of a distorted octahedron, and the band maximum at 481 nm is responsible for the orange color of the bulk oxide [58]. From

these data, it becomes clear that the position of the longest-wavelength CT band depends strongly on the coordination number of the central vanadium ion. It is also evident that this CT band shows a red shift when the coordination of the vanadium cation changes from tetrahedral to square pyramidal to octahedral.

In the present study, a very broad band centered at ca. 280 nm is observed for V-MCF samples with V loadings of up to 4.2 wt%. A deconvolution of this band reveals two main absorption features at 250 and 280 nm. On the basis of the Raman band at 1034 cm^{-1} (see Fig. 4), these features are assigned to isolated V sites in tetrahedral coordination. Moreover, the position of their band maxima is in good agreement with those of reference compounds for isolated VO_4. With increasing vanadium content, the intensity of the band at 280 nm increases with respect to the absorption appearing at 250 nm, resulting in a progressive shift of the overlapping band toward a higher wavelength. A similar shift of the absorption band at ca. 250 nm for mesoporous V-containing SBA-15 materials was reported earlier by our group [23]. The V-MCF samples with V loadings >4.2 wt% give rise to additional absorption bands at 300–400 nm, indicating the presence of polymerized VO_4 species. In addition, a new feature at 450 nm appears for the MCF samples with 5.6 wt% V loading, pointing to the presence of "bulk-like" V_2O_5 crystallites due to further polymerization of the V species [19,37,40].

Comparing the UV–vis spectrum of the dehydrated 4.2V-MCF catalyst with that obtained in its rehydrated state (Fig. 6, inset) shows that on hydration, a new band at 380 nm associated with pseudo-octahedrically coordinated V^{5+} species appears, indicating that most vanadium species in sample 4.2V-MCF are able to coordinate additional water molecules and thus are located in easily accessible sites. To extract the exact nature of different vanadia species and the symmetry environment of vanadium sites in the vanadium-containing MCF catalysts, absorption edge energy measurements were also performed by a procedure reported by Khodakov et al. [32]. The difference in edge energy values has been reported to depend on the support material and to the surface density of VO_x species [34]. In general, the edge energy values of the V^{4+} are in the 4.5–5 eV energy region, whereas the O^{2-} to V^{5+} ligand to metal charge transfer are in the 2–4 eV edge energy region [59]. From Table 1, it is apparent that all of the edge energy values are in the 2.3–3.3 eV range, and hence it is reasonable to assume that the tetrahedral-like V^{5+} species are the main surface vanadium species for V-MCF catalyst systems. Moreover, a careful examination of the four different V-silica systems shows that V-MCF catalyst produce a higher edge energy value than the reference systems supported on SBA-15, MCM-41, and conventional silica, thus pointing toward a decrease in the size or dimensionality of VO_x domains in the V-MCF systems [23,32–34].

H_2-TPR profiles of the catalysts taken at 200–800 °C show that the reduction onset temperature (T_{onset}), reduction temperature maxima (T_M), and the average oxidation state (AOS) values vary considerably in the V-MCF and V-SBA, V-MCM, and V-SiO_2 catalyst systems as given in Table 3 and illustrated in Fig. 7. The TPR profiles of the V-MCF catalysts exhibit only

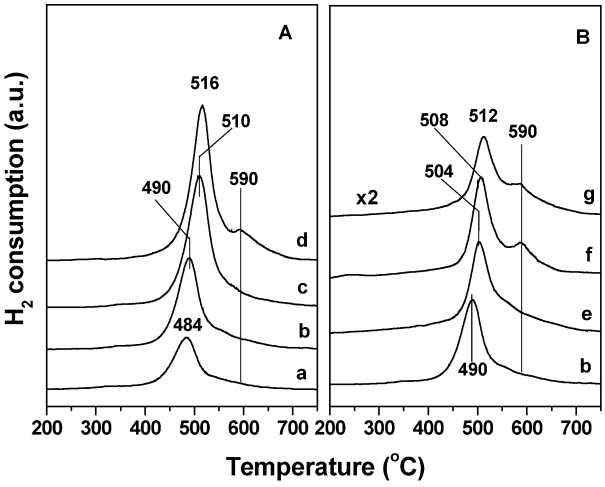

Fig. 7. H_2-TPR results of the mesoporous silica supported vanadium oxide catalysts: (a) 1.4V-MCF; (b) 2.8V-MCF; (c) 4.2V-MCF; (d) 5.6V-MCF; (e) 2.8V-SBA; (f) 4.2V-MCM; (g) 1.8V-SiO_2.

one sharp reduction peak at 480–510 °C, except in the case of the 5.6V-MCF sample, where an additional shoulder appears at ca. 590 °C. Whereas a progressive shift of the reduction maxima (T_M) of the main reduction peak to high temperature is observed for the V-MCF samples with increasing V loadings, an opposite trend for the onset temperature (T_{onset}) is identified. Obviously, the reducibility of the present V-MCF catalysts can be better reflected by the onset temperature, in good agreement with a progressive formation of easily reducible high-polymeric vanadium species at high V loadings [60]. By analogy with previous studies on the reducibility of VO_x/SiO_2 and other V-containing mesoporous materials [20,23,37,52], the peak at low temperature is attributed to the reduction of dispersed tetrahedral vanadium species, whereas the peak at 590 °C is attributed to the reduction of polymeric V^{5+} species V_2O_5-like.

In contrast, a close comparison of the profile for 2.8V-MCF sample with the profiles for 2.8V-SBA, 4.5V-MCM, and 1.8V-SiO_2 catalysts in Fig. 7b reveals that at the same V surface density level, the reduction temperature maxima (T_M) is much lower on the MCF catalyst than on its SBA-15, MCM-41, or conventional SiO_2 counterparts. In contrast to the single reduction feature of V-MCF and V-SBA samples, the V-MCM and V-SiO_2 catalysts show a distinct shoulder at ∼590 °C, indicating the formation of less-reducible "bulk-like" vanadia species, which may exist in a highly dispersed state on the support surface [37]. Moreover, the reduction onset temperature (T_{onset}) of the V-SBA, V-MCM, and V-SiO_2 materials is also significantly lower than that of the V-MCF sample, further confirming that the formation of highly dispersed vanadium species is favored over the surface of MCF. This finding is consistent with the results of UV–vis and Raman measurements reported above.

3.2. Catalytic tests in the ODH of propane

The activities of the V-MCF catalysts were explored under steady-state conditions at 450–650 °C with a constant GHSV (72,000 L kg_{cat}^{-1} h^{-1}) and propane/oxygen/nitrogen ratio (1:1:8).

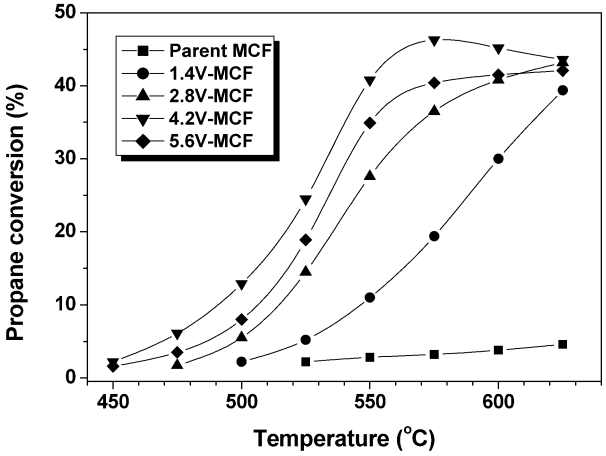

Fig. 8. Propane conversion as a function of temperature on V-MCF catalysts. (Reaction conditions: C_3H_8:O_2:N_2 = 1:1:8; GHSV = 72,000 L kg_{cat}^{-1} h^{-1}.)

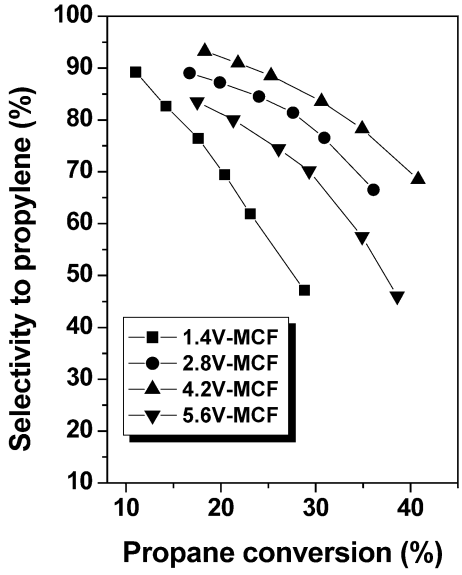

Fig. 9. Propylene selectivity as a function of propane conversion on V-MCF catalysts. (Reaction conditions: T = 550 °C; C_3H_8:O_2:N_2 = 1:1:8.)

Fig. 8 plots the ODH of propane on the V-MCF catalyst samples with varying vanadium content, as well as on the parent MCF as a function of reaction temperature. The figure shows that the catalytic activities of all of the V-MCF catalysts are highly dependent on the reaction temperature, and that propane conversion depends strongly on the vanadium content and increases rapidly with temperature. A 100% initial "jump" in conversion occurs when the V loading is increased from 1.4 to 2.8 wt%, and activity for the 4.2V-MCF catalyst is enhanced by 50%. This significant increase in conversion with loading can be attributed to the presence of high concentrations of isolated VO_x species fully accessible to reactants on the surface of 4.2V-MCF, as indicated by the characterization results. However, further increases in vanadium loading do not lead to increased propane conversion. Obviously, this negative loading effect on catalyst activity is due to the presence of polymerized vanadium species on the surface of 5.6V-MCF, for which a significant fraction of vanadium atoms is inaccessible to the reactants. Moreover, the 4.2V-MCF catalyst exhibits the maximum values of propane conversion in the entire temperature range studied, demonstrating the 4.2V-MCF sample's excellent performance for the oxidative transformation of propane.

Along with activity, selectivity to the corresponding light alkenes is also of paramount importance for the evaluation of ODH catalysts. Because selectivity is strongly related to conversion, a second series of experiments was conducted at constant temperature (550 °C) and varying GHSV (from 12,000 to 120,000 L kg_{cat}^{-1} h^{-1}), to attain different conversion levels. Propylene selectivity versus propane conversion is plotted in Fig. 9. Significant differences in the selectivity to propylene on the different V-containing MCF catalysts are observed. The 2.8V-MCF and 4.2V-MCF catalysts exhibit high selectivity (>65%) in the 0–40% conversion range and a continuous drop in selectivity for propylene with increasing conversion, due to secondary reactions of the olefin product. In comparison, a more pronounced decrease is seen for the 1.4V-MCF and 5.6V-MCF samples. It is also interesting that at all conversion levels, the selectivity to propylene shows a maximum on the catalyst with a vanadium content of 4.2 wt%. This finding is distinctly different from the results obtained over V-SBA-15 catalysts recently reported by our group [23], where the maximum selectivity toward olefin production was achieved with the V-SBA catalyst with a lower vanadium content of 2.8 wt%. Considering that the isolated surface vanadium species with tetrahedral coordination are the active and selective sites in the ODH reaction of propane, the present observation concerning the unique behavior of the selectivity to the desirable olefins products as a function of V loading clearly indicates that the vanadium surface density is a quite important parameter for tuning the reaction behavior of mesoporous supported vanadia species in the selective oxidation of propane.

The remarkable propane ODH activity, selectivity to propylene, turnover frequencies (TOFs) for propylene formation, and propylene productivity of the V-containing MCF catalysts are further indicated in Table 2. For comparison, the table also reports the catalytic results obtained on mesoporous SBA-15, MCM-41, and amorphous SiO_2-supported vanadia catalysts. Propylene, ethylene, CO, and CO_2 were the main reaction products formed on the different catalysts studied in this work. In addition, acrolein and trace amount of acetaldehyde were also detected (at total selectivity to these products <5%) with very minor differences among the samples studied. The results in Table 2 indicate that propane conversion at 550 °C depends strongly on the V content and the various supporting materials. Propylene is formed with high selectivity over the MCF catalysts with lower V content, and the propylene yield is much higher there than over conventional V/SiO_2 catalyst [17]. Table 2 also shows that the MCF catalysts with higher V content result in the formation of appreciable amounts of ethylene through the oxidative cracking pathway over V-MCF. Similar catalytic behavior was recently observed over V-catalysts supported on mesoporous silica, such as SBA-15 and HMS [23,24]. Note in particular that an excellent propene yield of 27.9% with a high $STY_{C_3H_6}$ of 3.77 kg propylene per kg_{cat}^{-1} h^{-1} was

Table 2
Oxidative dehydrogenation of propane on the mesoporous silica supported vanadia catalysts at 550 °C

Catalyst	C_3H_8 conv.[a] (%)	Selectivity (%)				C_3H_6 yield (%)	Light olefins yield[c] (%)	TOF × 10^{20} (μmol-C_3H_6 V^{-1} s^{-1})	$STY_{C_3H_6}$[d] (kg kg_{cat}^{-1} h^{-1})
		C_3H_6	C_2H_4	Oxygenates[b]	CO_x[c]				
MCF	2.8	68.8	11.5	–	16.3	1.9	2.2	–	0.26
1.4V-MCF	11.0	89.2	2.8	1.6	7.4	9.8	10.1	3.8	1.32
2.8V-MCF	27.6	81.4	5.7	1.7	11.2	22.5	24.0	4.3	3.04
4.2V-MCF	40.8	68.5	8.4	2.0	21.1	27.9	31.4	3.6	3.77
5.6V-MCF	34.9	57.5	10.3	1.6	28.9	20.1	23.7	1.9	2.71
2.8V-SBA	26.3	65.4	6.2	2.8	25.2	15.9	18.8	4.3	2.15
4.5V-MCM	24.2	55.3	5.3	3.1	36.3	13.4	14.7	2.3	1.81
1.8V-SiO_2	12.7	57.1	4.9	2.5	33.2	7.3	7.9	3.1	0.99

[a] Reaction conditions: $W = 0.05$ g, GHSV = 72,000 L kg_{cat}^{-1} h^{-1}, C_3H_8:O_2:N_2 = 1:1:8.
[b] Partial oxygenated products, i.e., acrolein and trace amount of acetaldehyde.
[c] CO_x products, i.e., CO_2 and CO; light olefins, i.e., C_3H_6 and C_2H_4.
[d] Rate of formation of propylene per unit mass of catalyst per time, $STY_{C_3H_6}$ (space-time yield) in kg kg_{cat}^{-1} h^{-1}.

Table 3
H_2-TPR results of the mesoporous silica supported vanadia catalysts

Sample	T_{onset}[a] (°C)	T_M[a] (°C)	H_2-uptake[b] (μmol-H_2 g^{-1})	AOS[b]
1.4V-MCF	401	484	216	4.55
2.8V-MCF	397	490	375	4.36
4.2V-MCF	393	510	462	4.12
5.6V-MCF	361	516	542	3.99
2.8V-SBA	340	504	352	4.28
4.5V-MCM	351	508	424	3.96
1.8V-SiO_2	337	512	160	4.02

[a] The onset temperature (T_{onset}) and the temperature of the maximum (T_M) hydrogen consumption.
[b] H_2 consumption in μmol-H_2 g^{-1} of catalyst and the average oxidation state (AOS) based on H_2 consumption.

obtained for the MCF catalyst with a V content of 4.2%, demonstrating attractive possibilities for industrial operations.

Up to now, the highest propylene yield in propane ODH, about 30%, was obtained with K–Mo catalysts highly dispersed on SiO_2/TiO_2 supports [7]. But this result was achieved with a very diluted feed, which leads to extremely low propylene productivity of no industrial interest. Generally, an industrially interesting space-time yield ($STY_{C_3H_6}$) is at least at 1 kg propylene per kg_{cat}^{-1} h^{-1} [61]. Table 2 shows that the $STY_{C_3H_6}$ obtained with the present V-containing MCF samples is well above this value, demonstrating the excellent performance of the V-MCF materials in the conversion of propane to propylene. The table also shows that the optimum performance in propane ODH occurs for 4.2V-MCF, which exhibits the highest rate of propylene production. Compared with the V-MCM and V/SiO_2 catalysts reported in the literature [19,20], our V-MCF catalyst exhibits much better propylene productivity for propane ODH.

It is also clear from Table 2 that the MCF with a large pore diameter and the interconnected 3D pore system is far superior to two-dimensional hexagonally ordered SBA-15 and MCM-41 as a support. With a similar V surface density, the 2.8V-MCF sample exhibited much higher C_3H_8 conversion and propylene yield than 2.8V-SBA, 4.5V-MCM, and 1.8V-SiO_2 catalysts. The high selectivity to propylene on the former at higher propane conversion levels can be related to the highly dispersed

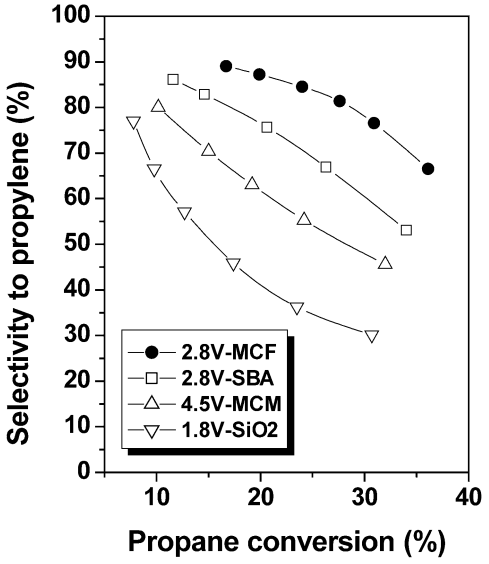

Fig. 10. Propylene selectivity as a function of propane conversion on various silica supported vanadia catalysts with a similar surface vanadium density. (Reaction conditions: $T = 550$ °C; C_3H_8:O_2:N_2 = 1:1:8.)

and isolated V anchored on the large surface of MCF with a much larger pore diameter and the well-defined 3D mesopore system as described above. It should be noted that the optimum V loading for the present V-MCF catalyst system is much higher than the V-loaded SBA-15 materials previously reported by our group [23]. In fact, a substantially lower V content of ca. 2.8 wt%, corresponding to nearly one-theoretical monolayer coverage (~0.69 VO_x per nm^2) of V atoms, is needed to attain the best ODH performance for V-SBA catalysts [23]. Higher surface density with high isolation of the active V species and more favorable conditions for mass transfer in the ODH of propane can be attributed to the enhanced catalytic performance of the V-MCF materials in the ODH of propane to propylene.

To provide further insight into the effect of support structure on the catalytic behavior of the V-containing silica materials, Fig. 10 compares the variation of the selectivity to propylene for the ODH of propane on various siliceous material-supported vanadium catalysts at the same V surface density level (~0.69 VO_x per nm^2). Apparently, the selectivity to propylene at both

low and high propane conversion levels decreases in the following sequence: 2.8V-MCF > 2.8V-SBA > 4.5V-MCM > 1.8V-SiO_2. By correlation with the textural data given in Table 1, the V-containing MCF catalyst with a well-defined 3D mesocellular porosity and ultra-large pore diameters is more selective than its SBA-15, MCM-41, and amorphous SiO_2 supported counterparts. It has been suggested that the MCF materials have an advantage over their more ordered counterparts MCM-41 or SBA-15 in terms of better diffusion properties, allowing the guest molecules to more readily access reactive centers that have been designed into the framework surfaces [26]. Moreover, a recent investigation of the ODH of propane over V-containing SBA-15 catalysts experimentally demonstrated that enhanced propylene selectivities at high propane conversions can be achieved with the V-SBA samples by providing more favorable conditions for mass transfer as compared with their MCM counterparts [23]. Taking into account all of these considerations, the superior catalytic performance of the present V-MCF catalyst can be reasonably attributed, in part, to its favorable molecular transport properties rendered by the unique mesocellular structure with ultra-large mesopore diameters of the MCF material, which can allow better diffusion of the produced propylene to the outside of the pore during the ODH of propane, consequently preventing subsequent deep oxidation.

4. Discussion

This work has investigated the use of a novel type of mesoporous siliceous MCF materials featuring a well-defined 3D, continuous, ultra-large mesopore structure as new promising support for the development of high-performance vanadium supported catalysts in the ODH of propane. The vanadium-supported MCF catalyst obtained by a simple alcoholic impregnation of NH_4VO_3 appears to be highly effective in the activation and selective conversion of propane to propylene at temperatures below 550 °C, offering propylene yields much higher than those provided by conventional vanadium catalysts in this reaction. Moreover, the excellent space-time yield, with up to 3.77 kg propylene per $kg_{cat}^{-1}\,h^{-1}$ for propylene production, makes the V-MCF catalyst systems very attractive for the ODH of propane from a technological standpoint, because the propylene productivity should be at least at 1 kg of propylene per $kg_{cat}^{-1}\,h^{-1}$ in potential industrial applications of such a process.

Spectroscopic characterization of MCF-supported VO_x as a function of loading, using Raman and UV–vis spectroscopy, revealed the presence of various VO_x surface structures (monomers, polymers, and crystals). At low vanadia loadings (<4.2 wt%), the surface is exclusively covered by isolated tetrahedral VO_4 species, whereas at higher loadings (4.2 wt%), besides isolated tetrahedral, chains of linked tetrahedra are present. At vanadia loadings >4.2 wt%, V_2O_5 crystallites are also observed. Previously reported results indicate that highly dispersed vanadium oxides on SBA-15 silica prepared by a novel alcoholic impregnation method can be generated with vanadia loadings up to 2.8 wt%, much higher than that needed for MCM-41 and conventional silica. In comparison, for the present VO_x/MCF samples prepared by the same alcoholic impregnation technique, spectroscopic characterization indicates the presence of polymeric species only at much higher loadings (4.2 wt% of V) and in very small concentrations.

Recently, the OH concentration of SBA-15 material (calcined at 500 °C) was determined to be 1.07 OH nm^{-2} [62]. Theoretically, this value can be considered a lower limit for the actual OH surface concentration in the present MCF samples used for the anchoring of VO_x, because they were used at ambient conditions without any temperature pretreatment. According to Zhuravlev [63,64], the silanol concentration of a fully hydroxylated silica surface amounts to 4.6 ± 0.5 OH nm^{-2}, which is claimed to be independent of the origin and characteristics (e.g., specific surface area, type of pores, pore size distribution) of the sample. DRIFTS spectra recorded for the V-MCF samples show that surface Si–OH hydroxyls are not fully consumed during deposition of 4.2 wt% of V (1.1 V nm^{-2}). Anchoring of these V atoms by formation of three-legged VO_4 species requires an OH surface concentration of ($3 \times 1.1 = 3.3$) OH nm^{-2}; therefore, it is reasonable that a higher amount of isolated and low-polymeric vanadium species on the MCF is achievable compared with the conventional silica support. However, the scission of some Si–O–Si siloxane bridges during the preparation process may also contribute to some extent to the anchoring of VO_x onto the surface of MCF support, as evidenced by the DRIFTS and Raman results.

In terms of catalytic performance, increasing the V loading was beneficial and boosted propane conversion as a consequence of a rise in the number of active VO_x sites, whereas propylene selectivity levels remained high (∼57%), even though appreciable amounts of low-polymeric vanadium species were formed on the catalyst surface. This indicates that both isolated and low-polymeric vanadium species are active and selective. Keep in mind that catalysts supported on two-dimensional hexagonally ordered siliceous SBA-15 and MCM-41, as well as on nonporous silica gel, were also tested in the reaction. The ODH performance of the 3D-structured V-MCF catalysts was much better than that of their conventional hexagonally ordered counterparts, inferring that apart from the active redox sites, the mass transfer properties of the catalyst also plays an important role in the gas-phase selective oxidation reactions.

Considering that the nature of the vanadium supported on siliceous materials is highly moisture sensitive [23,40], to gain a further insight into the impact of internal mass transfer properties on the adsorption or catalytic behavior of the V-containing silica materials, the rehydration of several separately prepared dehydrated V-silica materials was followed by UV resonance Raman spectroscopy, as shown in Fig. 11. The dehydrated samples obtained by dehydration under dry air at 550 °C exhibited Raman bands at 485, 1018, and 2036 cm^{-1}, associated with the vibration of the siloxane rings of siliceous support and fundamental-, as well as overtone V=O stretching of the isolated tetragonal vanadium species [23,31]. The absence of a typical band at ca. 990 cm^{-1} for V_2O_5 indicates that no free V_2O_5 phase was present and that the V was highly dispersed in all three mesoporous silica-based vanadia catalysts [65]. After hydration, exposing dehydrated samples to ambient air for

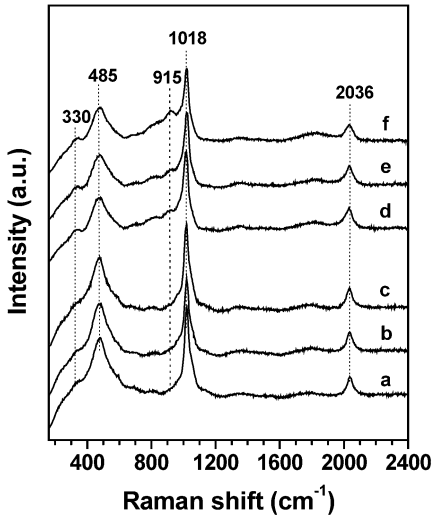

Fig. 11. In situ UV-Raman spectra of dehydrated (a, b, c) and rehydrated (d, e, f) 1.0V-MCM (a, d), 1.0V-SBA (b, e) and 1.0V-MCF (c, f) catalysts.

2 h led to two additional bands at 330 and 915 cm^{-1}, attributed to the stretching mode of V–OH_2 and V=O stretching coordinated with the H_2O molecule (H_2O–V=O), respectively, in the UV-Raman spectra [49]. Note that a variation in the relative intensity for H_2O–V=O stretching with respect to the tetrahedral V=O stretching band has been identified for the three hydrated samples, demonstrating the varying degrees of hydration of dispersed vanadia species achievable over the various mesostructured siliceous materials. It is clear that the isolated tetrahedral V species anchored on the pore walls of the siliceous MCF structure is more easily accessible to the water molecules at ambient conditions, as reflected by the more pronounced H_2O–V=O stretching observed for 1.0V-MCF, further demonstrating that the 3D continuous ultra-large mesopores of the MCF materials can readily allow much faster molecular transport during the ODH of propane.

Previous investigations concerning the use of vanadia-based catalysts for the ODH of propane have shown that various parameters, including oxidation state, coordination number, aggregation state and reducibility of vanadium species, distance between active sites, and acid/base properties and vanadium content of the catalysts, need to be considered to account for the catalytic behavior observed for the selective oxidation of propane [17–23]. Generally, catalysts with high vanadium dispersion show better performance in the selective oxidation of propane [17,23]. The presence of isolated tetrahedral V oxide species is essential for maintaining high conversion and selectivity in the ODH of propane, whereas polymeric vanadium species could favor undesired combustion reaction pathways, leading to the formation of carbon oxides. Kaliaguine et al. recently described the use of MCF materials as promising supports for preparation of a new type of TS-1 zeolite–coated mesoporous materials that exhibit high specific activity in the liquid-phase selective hydroxylation of a bulky molecule 1-naphthol compared with their conventional TS-1 counterparts [28]. In the present work, we have unambiguously demonstrated the unique advantage of MCF materials as new, promising supports for the generation of novel V-containing MCF materials with favorable molecular transport properties for the ODH of propane (Fig. 12). Our results confirms that although the creation of active redox sites is a prerequisite for the gas-phase selective oxidation of propane, it does not completely account for the observed changes in activity and selectivity; the molecular transport properties of the catalyst must be taken into account.

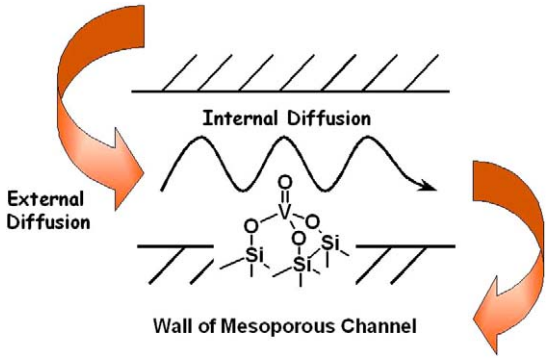

Fig. 12. Schematic illustration of the molecular transport effect on V-containing mesoporous catalysts during the oxidative dehydrogenation of propane.

5. Conclusion

This study has demonstrated that MCF materials are new, attractive supports applicable for the fabrication of promising V-MCF catalysts that are highly active and selective for the ODH of propane. The results show that the V-containing MCF catalysts have a unique textural structure with high surface area along with well-defined 3D mesocellular porosity and ultra-large pore diameters. Comparisons with V-MCF, V-SBA-15, V-MCM-41, and conventional V–SiO_2 catalysts demonstrate that a much higher concentration of isolated V species easily accessible to the reactants is readily achievable on the surface of the MCF support. Moreover, a much weaker and lower acidity of the surface acid sites are observed for the vanadium-incorporated MCF catalysts. The superior performance of the present mesoporous VO_x/MCF catalysts in the ODH of propane has been attributed to the well-defined 3D mesopore systems and the much larger pore diameters of the MCF materials. As a result, the ODH of propane could proceed much more effectively over the V-containing MCF catalysts with a higher concentration of isolated VO_x species and favorable conditions for internal mass transfer, thereby leading to the significant enhancement of their performance in the ODH of propane.

Acknowledgments

This work was supported by the National Natural Science Foundation of China (Grants 20421303, 20473021, 20503005, and 20407006), the National Key Basic Research Program (Grant 2003CB615807), and the Research Fund for the Doctoral Program of Higher Education (Grant 20050246071).

References

[1] B.K. Warren, S.T. Oyama, Heterogeneous Hydrocarbon Oxidation, vol. 638, Am. Chem. Soc., Washington, DC, 1996.
[2] D. Vitry, J.-L. Dubois, W. Ueda, J. Mol. Catal. A 220 (2004) 67.
[3] A.H. Tullo, Chem. Eng. News 81 (2003) 21.
[4] M.M. Bettahar, G. Costentin, L. Savary, J.C. Lavalley, Appl. Catal. A 145 (1996) 1.
[5] M. Chaar, D. Patel, M. Kung, H.H. Kung, J. Catal. 109 (1988) 463.
[6] T. Blasco, J.M.L. Nieto, Appl. Catal. A 157 (1997) 117.
[7] R.B. Watson, U.S. Ozkan, J. Catal. 191 (2000) 12.
[8] J. Jarupatrakorn, T.D. Tilley, J. Am. Chem. Soc. 124 (2002) 8380.
[9] C. Mazzochia, C. Aboumrad, C. Diage, E. Tempesti, J.M. Herrmann, G. Thomas, Catal. Lett. 10 (1991) 181.
[10] M. Chaar, D. Patel, M. Kung, H.H. Kung, J. Catal. 109 (1988) 463.
[11] R.H.H. Smits, K. Seshan, H. Leemreize, J.R.H. Ross, Catal. Today 16 (1993) 513.
[12] Y.S. Yoon, W. Ueda, Y. Moro-oka, Top. Catal. 3 (1996) 265.
[13] F. Cavani, F. Trifirò, Catal. Today 24 (1995) 307.
[14] G. Centi, F. Trifirò, Appl. Catal. A 143 (1996) 3.
[15] J.S. Beck, J.C. Vartuli, W.J. Roth, M.E. Leonowicz, C.T. Kresge, K.D. Schmitt, C.T.W. Chu, D.H. Olsen, E.W. Sheppard, S.B. McCullen, J.B. Higgins, J.L. Schlenker, J. Am. Chem. Soc. 114 (1992) 10834.
[16] A. Corma, Chem. Rev. 97 (1997) 2373.
[17] M.L. Peña, A. Dejoz, V. Fornés, E. Rey, M.I. Vázquez, J.M. López Nieto, Appl. Catal. A 209 (2001) 155.
[18] O.V. Buyevskaya, A. Bruckner, E.V. Kondratenko, D. Wolf, M. Baerns, Catal. Today 67 (2001) 369.
[19] B. Solsona, T. Blasco, J.M.L. Nieto, M.L. Pena, F. Rey, A. Vidal-Moya, J. Catal. 203 (2001) 443.
[20] J. Santamaria-Gonzalez, J. Luque-Zambrana, J. Merida-Robles, P. Maireles-Torres, E. Rodriguez-Castellon, A. Jimenez-Lopez, Catal. Lett. 68 (2000) 67.
[21] Y.M. Liu, Y. Cao, K.K. Zhu, S.R. Yan, W.L. Dai, H.Y. He, K.N. Fan, Chem. Commun. (2002) 2832.
[22] Y.M. Liu, Y. Cao, S.R. Yan, W.L. Dai, K.N. Fan, Catal. Lett. 88 (2003) 61.
[23] Y.M. Liu, Y. Cao, K.K. Zhu, S.R. Yan, W.L. Dai, H.Y. He, K.N. Fan, J. Catal. 224 (2004) 417.
[24] P. Schmidt-Winkel, W.W. Lukens Jr., D. Zhao, P. Yang, B.F. Chmelka, G.D. Stucky, J. Am. Chem. Soc. 121 (1999) 254.
[25] J.S. Lettow, Y.J. Han, P. Schmidt-Winkel, P. Yang, D. Zhao, G.D. Stucky, J.Y. Ying, Langmuir 16 (2000) 8291.
[26] D.T. On, S. Kaliaguine, J. Am. Chem. Soc. 125 (2003) 618.
[27] Y.J. Han, J.T. Watson, G.D. Stucky, A. Butler, J. Mol. Catal. B 17 (2002) 1.
[28] D. Trong On, A. Ungureanu, S. Kaliaguine, Phys. Chem. Chem. Phys. 5 (2003) 3534.
[29] A. Ungureanu, D. Trong On, E. Dumitriu, S. Kaliaguine, Appl. Catal. A 254 (2003) 203.
[30] P. Kuśtrowski, L. Chmielarz, R. Dziembaj, P. Cool, E.F. Vansant, J. Phys. Chem. B 109 (2005) 11552.
[31] R. Zhou, Y. Cao, S.R. Yan, J.F. Deng, Y.Y. Liao, B.F. Hong, Catal. Lett. 75 (2001) 107.
[32] A. Khodakov, J. Yang, S. Su, E. Iglesia, A.T. Bell, J. Catal. 177 (1998) 343.
[33] A. Khodakov, B. Olthof, A.T. Bell, E. Iglesia, J. Catal. 181 (1999) 205.
[34] A. Davydov, in: N.T. Sheppard (Ed.), Molecular Spectroscopy of Oxide Catalyst Surfaces, Wiley, Chichester, 2003, p. 5.
[35] P. Schmidt-Winkel, W.W. Lukens Jr., P. Yang, D.I. Margolese, J.S. Lettow, J.Y. Ying, G.D. Stucky, Chem. Mater. 12 (2000) 686.
[36] L.A. Feigin, D.I. Svergun, Structure Analysis by Small-Angle X-Ray and Neutron Scattering, Plenum, New York, 1987.
[37] H. Berndt, A. Martin, A. Brückner, E. Schreier, D. Müller, H. Kosslick, G.-U. Wolf, B. Lücke, J. Catal. 191 (2000) 384.
[38] M. Morey, A. Davidson, H. Eckert, G. Stucky, Chem. Mater. 8 (1996) 486.
[39] E. Geidel, H. Lechert, J. Döbler, H. Jobic, G. Calzaferri, F. Bauer, Microporous Mesoporous Mater. 65 (2003) 31.
[40] D. Wei, H. Wang, X. Feng, W.T. Chueh, P. Ravikovitch, M. Lyubovsky, C. Li, T. Takeguchi, G.L. Haller, J. Phys. Chem. B 103 (1999) 2113.
[41] C.B. Wang, G. Deo, I.E. Wachs, J. Catal. 178 (1998) 640.
[42] N. Das, H. Eckert, H. Hu, I.E. Wachs, J.F. Walzer, F.J. Feher, J. Phys. Chem. 97 (1993) 8240.
[43] G.T. Went, S.T. Oyama, A.T. Bell, J. Phys. Chem. 94 (1990) 4240.
[44] K.J. Chao, C.N. Wu, H. Chang, L.J. Lee, S.F. Hu, J. Phys. Chem. B 101 (1997) 6341.
[45] R. Rulkens, J.L. Male, K.W. Terry, B. Olthof, A. Khodakov, A.T. Bell, E. Iglesia, T.D. Tilley, Chem. Mater. 11 (1999) 2966.
[46] K.L. Walther, M. Schraml-Marth, A. Wokaun, A. Baiker, Catal. Lett. 4 (1990) 327.
[47] Z.H. Luan, P.A. Meloni, R.S. Czernuszewicz, L. Kevan, J. Phys. Chem. B 101 (1997) 9046.
[48] P. McMillan, Am. Mineral. 69 (1986) 622.
[49] X. Gao, S.R. Bare, B. Weckhuysen, I.E. Wachs, J. Phys. Chem. B 102 (1998) 10842.
[50] S. Xie, E. Iglesia, A.T. Bell, Langmuir 16 (2000) 7162.
[51] A.J. Van Hengstum, J.G. Van Ommen, H. Bosch, P.J. Gellings, Appl. Catal. 5 (1983) 207.
[52] M. Baltes, K. Cassiers, P. Van der Voort, B.M. Weckhuysen, R.A. Schoonheydt, E.F. Vansant, J. Catal. 197 (2001) 160.
[53] S.M. Chraml-Marth, A. Wokaun, M. Pohl, H.L. Krauss, J. Chem. Soc., Faraday Trans. 87 (1991) 2635.
[54] U. Scharf, M. Schraml-Marth, A. Wokaun, A. Baiker, J. Chem. Soc., Faraday Trans. 87 (1991) 3299.
[55] M. Nabavi, F. Taulelle, C. Sanchez, M. Verdaguer, J. Phys. Chem. Solids 51 (1990) 1375.
[56] H.T. Evans, Z. Krystallogr. 114 (1960) 257.
[57] F. Marumo, M. Isobe, S. Iwai, Y. Kondo, Acta Crystallogr. B 30 (1974) 1628.
[58] G. Centi, S. Perathoner, F. Trifiro, A. Aboukais, C.F. Aissi, M. Guelton, J. Phys. Chem. 96 (1992) 2617.
[59] H. So, M.T. Pope, Inorg. Chem. 11 (1972) 1441.
[60] S. Shylesh, A.P. Singh, J. Catal. 228 (2004) 333.
[61] J.B. Stelzer, J. Caro, M. Fait, Catal. Commun. 6 (2005) 1.
[62] K.L. Fujdala, T.D. Tilley, J. Am. Chem. Soc. 123 (2001) 10133.
[63] L.T. Zhuravlev, Langmuir 3 (1987) 316.
[64] L.T. Zhuravlev, Colloids Surf. A 74 (1993) 71.
[65] G. Xiong, C. Li, H.Y. Li, Q. Xin, Z. Feng, Chem. Commun. (2000) 677.